Target-Driven Positive Selection at Hot Spots of Scorpion Toxins Uncovers Their Potential in Design of Insecticides

Limei Zhu,[1] Steve Peigneur,[2] Bin Gao,[1] Shangfei Zhang,[1] Jan Tytgat,[2] and Shunyi Zhu*[,1]

[1]Group of Peptide Biology and Evolution, State Key Laboratory of Integrated Management of Pest Insects & Rodents, Institute of Zoology, Chinese Academy of Sciences, Beijing, China

[2]Laboratory of Toxicology, University of Leuven, Leuven, Belgium

***Corresponding author:** E-mail: zhusy@ioz.ac.cn.

Associate editor: Miriam Barlow

Abstract

Positive selection sites (PSSs), a class of amino acid sites with an excess of nonsynonymous to synonymous substitutions, are indicators of adaptive molecular evolution and have been detected in many protein families involved in a diversity of biological processes by statistical approaches. However, few studies are conducted to evaluate their functional significance and the driving force behind the evolution (i.e., agent of selection). Scorpion α-toxins are a class of multigene family of peptide neurotoxins affecting voltage-gated Na^+ (Na_v) channels, whose members exhibit differential potency and preference for insect and mammalian Na_v channels. In this study, we undertook a systematical molecular dissection of nearly all the PSSs newly characterized in the *Mesobuthus* α-toxin family and a two-residue insertion (^{19}AlaPhe^{20}) located within a positively selected loop via mutational analysis of α-like MeuNaTxα-5, one member affecting both insect and mammalian Na_v channels. This allows to identify hot-spot residues on its functional face involved in interaction with the receptor site of Na_v channels, which comprises two PSSs (Ile^{40} and Leu^{41}) and the small insertion, both located on two spatially separated functional loops. Mutations at these hot-spots resulted in a remarkably decreased anti-mammalian activity in MeuNaTxα-5 with partially impaired or enhanced insecticide activity, suggesting the potential of PSSs in designing promising candidate insecticides from scorpion α-like toxins. Based on an experiment-guided toxin-channel complex model and high evolutionary variability in the receptor site of predators and prey of scorpions, we provide new evidence for target-driven adaptive evolution of scorpion toxins to deal with their targets' diversity.

Key words: **electrophysiological recording, predation, prey, selective agent, sodium channel, toxin-channel complex.**

Introduction

Identifying individual codons that undergo accelerated substitutions is evidence for adaptive evolution of proteins. Statistics-based methods have revealed many such examples in neurotoxins from a diversity of venomous animals, such as hanatoxins from spiders, conotoxins and A-superfamily of conopeptides from cone snails, a variety of ion channel-targeted toxins from scorpions, and phospholipase A2 serine proteinases from snakes (Duda and Palumbi 1999, 2000; Zhu et al. 2005; Juárez et al. 2008; Tian, Yuan, et al. 2008; Puillandre et al. 2010; Kozminsky-Atias and Zilberberg 2012; Wang et al. 2012; Wong and Belov 2012; Vonk et al. 2013). This is presumably due to a need for coevolution with their prey and predators. Only recently, people began to make efforts to explore functional significance of these accelerated substitution sites (also termed positive selection sites, PSSs) in specific toxin families (Weinberger et al. 2010; Wang et al. 2012), which demonstrated the usefulness of evolutionary information combined with site-directed mutagenesis in rapidly identifying functional sites of animal toxins.

Scorpion toxins affecting voltage-gated sodium (Na_v) channels (abbreviated as ScNaTxs) are a large family of toxic peptides with a conserved cysteine-stabilized α-helix and β-sheet fold cross-linked by four disulfide bridges (Possani et al. 1999). These toxins are classified into two distinct types (α and β) based on their pharmacological effects and channel binding properties (Jover et al. 1980; Cestele and Catterall 2000). Alpha-ScNaTxs bind to receptor site 3 of Na_v channels in a voltage-dependent manner. Site 3 is composed of a primary site comprising two extracellular loops linking S1–S2 and S3–S4 fragments in domain IV of Na_v channels that is located in the voltage sensor domain (herein called VSD (IV)), and a secondary site located on the pore module of domain I (Cestele and Catterall 2000). Such binding prevents the outward movement of the DIV-S4, the S4 segment in domain IV of Na_v channels, necessary for the rapid inactivation of the channels (Cestele and Catterall 2000; Bosmans and Tytgat 2007). Extensive mutational analyses of different α-ScNaTxs (e.g., BmKM1 from *Mesobuthus martensii* Karsch; Lqh2, Lqh3, and LqhαIT from *Leiurus quinquestriatus hebraeus*) have highlighted their bipartite functional surfaces comprising a core-domain and an NC-domain (Wang et al. 2003; Karbat et al. 2004, 2007; Gordon et al. 2007; Kahn et al. 2009). The core-domain is formed by residues at the loops connecting secondary structure elements of the toxins and interacts with the primary site; and the NC-domain is composed of an amino-terminal five-residue turn (N-turn) and the carboxyl-

Article

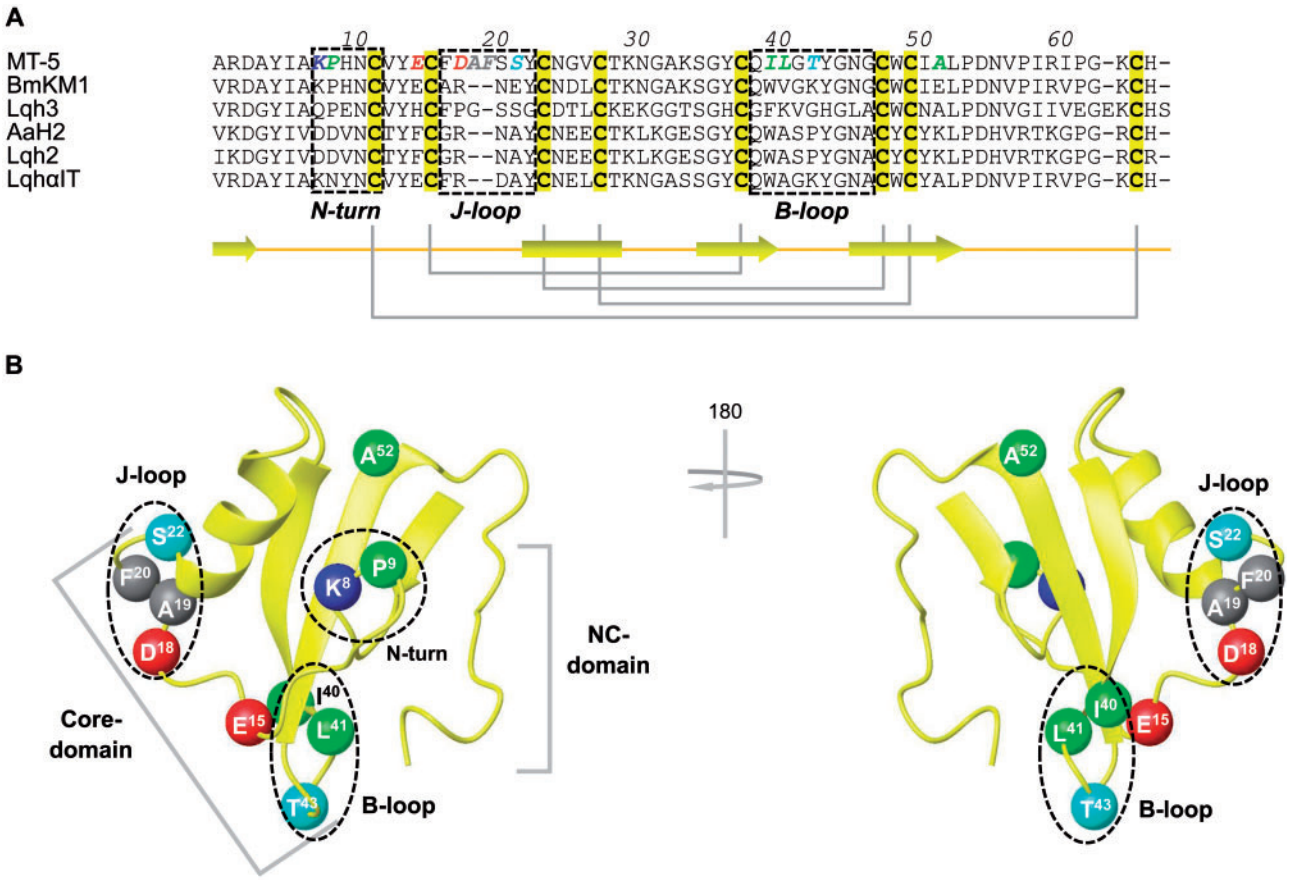

FIG. 1. Location of PSSs on the structure of MT-5. (*A*) Multiple sequence alignment of MT-5 and other α-ScNaTxs with functional sites known. Secondary structure elements are extracted from the experimental structure of MT-5. Cysteines forming disulfide bonds are shadowed in yellow and regions (N-turn and two loops) under PS are boxed. Nine PSSs are italicized and differently colored based on their side-chain characteristics (Acidic, red; basic, blue; hydrophobic, green; hydrophilic, cyan). *Mesobuthus eupeus*-specific two-residue insertion in J-loop is colored in gray. (*B*) Mapping of the PSSs and the lineage-specific insertion of J-loop (A^{19} and F^{20}) on MT-5. The residues are represented by their Cα atoms in sphere with consistent color codes to those in figure 1A. The N-turn and two loops are circled.

tail (C-tail), which interacts with the secondary site (Zhang et al. 2015, 2016). On the basis of preferential toxicity to mammals or insects, α-ScNaTxs are further divided into three pharmacological subgroups: classical α-toxins bind with high affinity to mammalian brain Na_v channels and are practically nontoxic to insects (e.g., AaH2 from *Androctonus australis* and Lqh2) whereas anti-insect α-toxins are highly toxic to insects but low potent to mammals (e.g., LqhαIT and MeuNaTxα-4 from *M. eupeus*). Alpha-like toxins are highly active on both mammals and insects (e.g., BmKM1 and Lqh3) (Bosmans and Tytgat 2007; Gordon et al. 2007; Zhu et al. 2012).

As essential lethal components of scorpion venom in capturing prey (e.g., arthropods) and repelling predators (e.g., birds, lizards, and small mammals; Polis 1990), the α-ScNaTx family has evolved under strong positive selection (PS, also known as positive Darwinian selection) and is emerging as a research model of toxin evolution owing to small variations at the interface of toxins and Na_v channels resulting in significant difference in potency and selectivity (Gordon and Gurevitz 2003; Gordon et al. 2007). Since the first report on PS of α-ScNaTxs (Zhu et al. 2004), at least three other papers have been published (Weinberger et al. 2010; Kozminsky-Atias and Zilberberg 2012; Zhu et al. 2012). All these studies detected PS signals and indicated that many PSSs are located on functional regions of the toxins. Despite a similar statistical approach used in these studies, PSSs detected exhibited some differences. For example, Zhu et al. (2004) detected seven PSSs based on a small data set, of which six are located on functional surfaces of different toxins. Six years later, Weinberger et al. (2010) identified four PSSs based on a larger data set from a diversity of scorpion species, which are nested in the seven PSSs and are also functionally important. This work provides an example of mutations at PSSs improving the potency and selectivity of α-ScNaTxs (Weinberger et al. 2010). More recently, we analyzed a total of 34 sequences of α-ScNaTxs from two sibling species of *Mesobuthus* (*M. eupeus* and *M. martensii*) and detected nine PSSs, of which six were unique in this analysis and the majority of them being located on the N-turn and two structural loops (B- and J-loop) (Zhu et al. 2012; fig. 1).

Given that accelerated amino acid substitutions are selectively favored (Morgan et al. 2012), we thus assume that these PSSs could contribute to the functional role of the *Mesobuthus* α-ScNaTxs. To verify this assumption, we carried out a systematical mutational analysis of nearly all the PSSs in an α-like toxin from *M. eupeus* (MeuNaTxα-5, abbreviated as

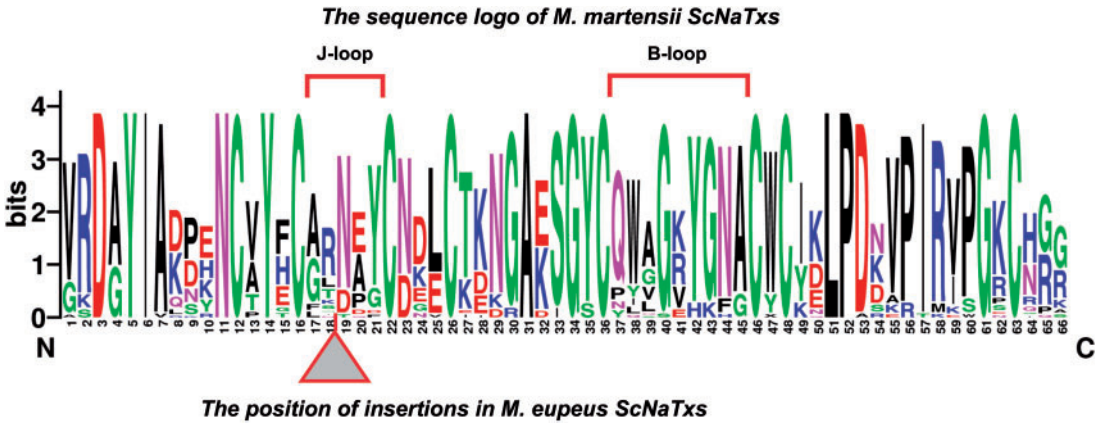

FIG. 2. The sequence logo of *M. martensii ScNaTxs*. The logo was created from 33 sequences of *M. martensii* ScNaTxs (supplementary table S1, Supplementary Material online) by WebLogo, a web-based tool for creating sequence logos from multiple sequence alignment (Crooks et al. 2004). The triangle indicates the position of insertion in *M. eupeus* ScNaTxs (Zhu et al. 2012). Two positively selected loops are labeled here.

MT-5) by introducing small side-chains (i.e., alanine or glycine) and deleting a *M. eupeus*-specific two-amino acid insertion (^{19}AF^{20}) in a positively selected loop (J-loop) (figs. 1 and 2). Two-electrode voltage clamp and in vivo toxicity assay were used to compare the change in activity between MT-5 and its mutants. Our results show that PSSs located in two positively selected loops are involved in the direct interaction with the receptor site of Na_v channels, in which two PSSs and the insertion constitute hot spots of the toxin-channel interface. A combination of sequence, structural, and functional data provides new evidence for the role of the toxin-bound region of Na_v channels from both predators and prey of scorpions in driving PS of hot-spot residues of the toxins. A series of mutants of MT-5 with selective insect toxicity is also reported.

Results

Design of Mutations

A PSS is a site with the ratio of the number of nonsynonymous substitutions per nonsynonymous site (d_N) to the number of synonymous substitutions per synonymous site (d_S) (i.e., ω) > 1 (Hill and Hastie 1987; Hughes and Nei 1988). In our previous studies, we have identified nine PSSs in two multigene families of ScNaTxs (*M. eupeus* and *M. martensii*), including sites 8, 9, 15, 18, 22, 40, 41, 43, and 52 (numbered according to MT-5, corresponding to sites 8, 9, 15, 18, 20, 38, 39, 41, and 50 in BmKM1) (Zhu et al. 2012), in which three (18, 41, and 43) were common to previous analyses from different sequence data sets (Weinberger et al. 2010; Zhu et al. 2012) and others were specific in this analysis. In spite of the difference in position, structurally, PSSs predicted from different data sets are similarly located in three main regions: the N-turn, the J-loop (a region preceding the α-helix), and the B-loop (a region located between the second and third β-strands, except site 52 that is situated on the end of the last β-strand (Zhu et al. 2012; fig. 1). This suggests that these toxins originating from different scorpion species might have undergone similar selective pressure during evolution.

To investigate the functional significance of the PSSs, we designed a series of mutants of MT-5 with these PSSs replaced by small amino acids, Ala or Gly, except site 52 that is occupied by an alanine and thus a Lys (A52K) was introduced. Considering a key functional role of the J-loop in ScNaTxs (e.g., Lqh2, Lqh3, and LqhαIT) (Zhu et al. 2012) and the abundance of PSSs in this loop (fig. 1A), we deleted a *M. eupeus*-specific two-residue-insertion located in this positively selected loop (^{19}AF^{20}) (figs. 1 and 2) to observe the potential impact of this small insertion on toxin's function. The choice of MT-5 as a representative is based on the availability of its experimental 3D structure and pharmacological functional data (Zhu et al. 2012). Primers for constructing the mutants mentioned above by inverse polymerase chain reaction (PCR) are listed in the table 1.

Identification of Recombinant Peptides

According to the method of preparation of recombinant MeuNaTxα-12 and MeuNaTxα-13 in *Escherichia coli* (Zhu et al. 2013), we firstly obtained highly pure recombinant MT-5 (rMT-5), as identified by reverse phase high-performance liquid chromatography (RP-HPLC) and matrix-assisted laser desorption/ionization time of flight (MALDI-TOF). The peptide was eluted as a single peak at 25 min (fig. 3A) and its experimental molecular weight of 7,171.4 Da matched its theoretical mass of 7,171.2 Da (table 2), indicating that four disulfide bonds have been formed and the extra N-terminal Met has been automatically removed during purification, as in the case of MeuNaTxα-12 and MeuNaTxα-13 (Zhu et al. 2013). Subsequently, we constructed a series of rMT-5 mutants to cover all the PSSs and a deletion mutant (Δ^{19}AF^{20}). All mutants except T43A were expressed as inclusion bodies in *E. coli*. For T43A, only a small amount of product was available, which hampered further refolding and purification. All refolded mutants were finally purified by RP-HPLC and their experimental weights were determined by MALDI-TOF (table 2).

Effect of MT-5 and Mutants on Na_v channels

First, we assessed the effect of rMT-5 on five mammalian Na_v channel subtypes (i.e., rNa_v1.1, rNa_v1.2, rNa_v1.4, rNa_v1.5, and mNa_v1.6) and the *Drosophila* counterpart (*Dm*Na_v1)

Table 1. Primers Used in This Study.

Gene	Primer Name	Sequence
rMT-5	MeuNaTxα-12/13F[a]	5′-CCATGGCTCGTGATGCYTATATT -3′
	MeuNaTxα-13R[a]	5′-GTCGACTTAATGGCATTTTCCTGGTAT-3′
K8A	K8A-F	5′-*GC*GCCCCATAACTGTGTATACGAA-3′
	K8A/P9A-R[b]	5′-GGCAATATAAGCATCACGAGCCAT-3′
P9A	P9A-F	5′-AAGGC*G*CATAACTGTGTATACGAA-3′
	K8A/P9A-R[b]	5′-GGCAATATAAGCATCACGAGCCAT-3′
E15A	E15A-F	5′-*GC*GTGTTTTGATGCATTTAGTAGT-3′
	E15A-R	5′-GTATACACAGTTATGGGGCTTGGC-3′
D18A	D18A-F	5′-*GC*GGCATTTAGTAGTTATTGCAAC-3′
	D18A-R	5′-AAAACATTCGTATACACAGTTATG-3′
S22G	S22G-F	5′-*GG*CTATTGCAACGGTGTATGTACC-3′
	S22G-R	5′-ACTAAATGCATCAAAACATTCGTA-3′
I40A	I40A-F	5′-*GC*GCTCGGTACATATGGAAATGGT-3′
	I40A/L41A-R[b]	5′-TTGGCAATAGCCACTCTTAGCACC-3′
L41A	L41A-F	5′-ATC*GC*GGGTACATATGGAAATGGT-3′
	I40A/L41A-R[b]	5′-TTGGCAATAGCCACTCTTAGCACC-3′
T43A	T43A-F	5′-GC*G*TATGGAAATGGTTGCTGGTGC-3′
	T43A-R	5′-ACCGAGGATTTGGCAATAGCCACT-3′
A52K	A52K-F	5′-*AA*ATTGCCCGATAATGTACCGATTAGA-3′
	A52K-R	5′-TATGCACCAGCAACCATTTCCATATGT-3′
Δ19AF20	DelAF-F	5′-AGTAGTTATTGCAACGGTGTATGT-3′
	DelAF-R	5′-ATCAAAACATTCGTATACACAGTT-3′

NOTE.—Mutated codons are italics and restriction endonuclease sites (Nco I and Sal I) underlined once. All primers listed here were synthesized by SBS Genetech (Beijing, China).
[a]Primers previously published, in which "Y" means "T or C" (Zhu et al. 2013).
[b]Reverse primers shared by two mutants.

expressed in *Xenopus* oocytes, in which except $rNa_v1.1$, others had been evaluated previously for native MT-5 (Zhu et al. 2012). In these mammalian channels, $rNa_v1.1$, $rNa_v1.2$, and $rNa_v1.6$ are primarily expressed in brain; $rNa_v1.4$ in muscle; and $Na_v1.5$ in heart (Catterall et al. 2005). The results showed that rMT-5 had identical channel spectrum to the native peptide (Zhu et al. 2012; fig. 3B), in which $rNa_v1.2$ was the only one resistant channel. rMT-5 slowed rapid inactivation of the sensitive Na_v channels with preference for $DmNa_v1$ and $rNa_v1.1$. The high efficacy of rMT-5 on these two channels was also reflected by their I_{30ms}/I_{peak} (2.5 and 0.6, respectively; table 2). The 50% effective concentration (EC_{50}) determined here was 0.34 ± 0.05 μM for $DmNa_v1$, nearly consistent with that of the native peptide (0.28 ± 0.04 μM) (Zhu et al. 2012). The EC_{50} was 0.45 ± 0.15 μM for $rNa_v1.1$ (table 3). $rNa_v1.1$ and $DmNa_v1$ were thus chosen for further assaying mutational effect at the PSSs. As shown in figure 4A, among the nine mutants, six (K8A, P9A, E15A, D18A, S22G, and A52K) retained or partly retained their activity on $Na_v1.1$ at 1 μM, whereas at the same concentration three (I40A, L41A, and Δ19AF20) completely lost activity (fig. 4A). To quantitatively compare the potency of the mutants, we determined EC_{50} values of the six mutants according to the published procedures (Zhu et al. 2012; fig. 5 and table 3). EC_{50} values of I40A, L41A, and Δ19AF20 were not determined because they showed no detectable effect or minor effect even at a peptide concentration greater than 50 μM (fig. 5), indicating that they serve as hot-spot residues implicated in binding to the channel. Overall, the activity of E15A, D18A, S22G, and A52K was decreased by about 3- to 5-fold, whereas K8A and P9A retained a similar activity to rMT-5. Interestingly, despite significantly decreased activity in most of MT-5 mutants on $Na_v1.1$, all mutants did exhibit similar activity on $DmNa_v1$ as compared to the unmodified peptide (fig. 4B), with EC_{50} values of 0.3–0.4 μM (table 3).

To investigate the effect of the mutations on other channel subtypes, we assessed the pharmacological activity of the mutants on $rNa_v1.2$, $rNa_v1.4$, and $mNa_v1.6$ (fig. 6). The majority of the mutants, including both nonhot-spots and hot-spots, and the unmodified peptide, were inactive to $rNa_v1.2$ at 10 μM, with the exception of S22G that gained some weak activity on $rNa_v1.2$ at this concentration (fig. 6A), suggesting that mutation at a PSS may alter the channel selectivity in some cases. At a higher concentration (50 μM), the three hot-spot mutants still lacked activity on $rNa_v1.2$. For $rNa_v1.4$ and $mNa_v1.6$, we observed similar results, as in the case of $rNa_v1.1$. Mutations at these three hot-spots significantly decreased the activity on these two channels (fig. 6B). It is remarkable that nearly all mutants apart from P9A at the nonhot-spots showed significant activity on $rNa_v1.4$ at 10 μM (fig. 6A) but at the same concentration, this channel showed resistance on the three hot-spot mutants, and at 5-fold higher concentration (50 μM) only weak activity was observed (fig. 6B). A similar case was also found in $mNa_v1.6$. At 1 μM, all the nonhot-spot mutants retained activity but only weak activity appeared in L41A and Δ19AF20 at a higher concentration (fig. 6B). We also noted that although the activity on $rNa_v1.1$ and $mNa_v1.6$ was retained in P9A, its activity on $rNa_v1.4$ was lost (fig. 6A), suggesting differential functional importance of this PSS in binding to different Na_v channel subtypes.

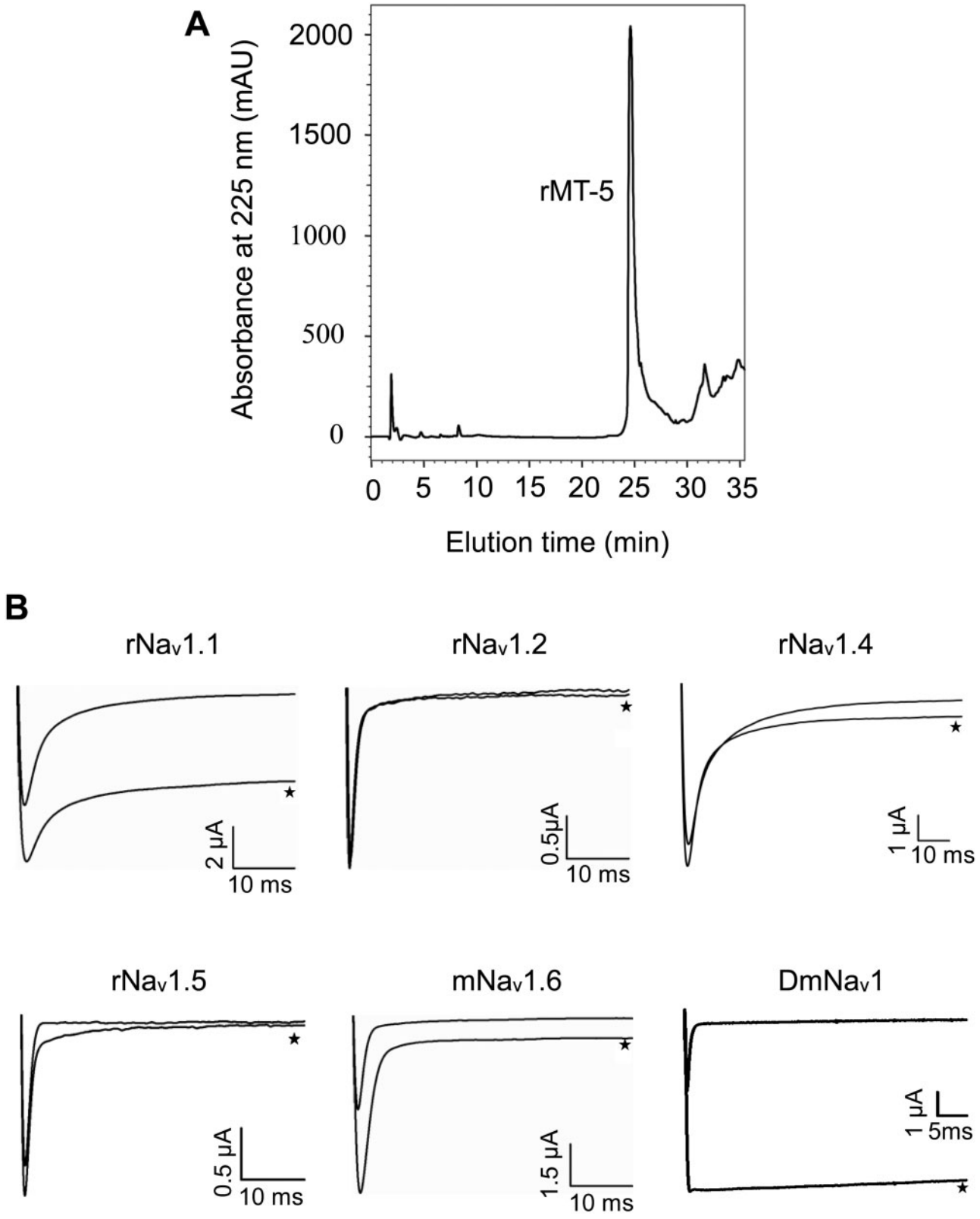

FIG. 3. Purification and functional characterization of rMT-5. (*A*) RP-HPLC showing retention time of rMT-5. C18 column (Agilent Zorbax 300SB-C18, 4.6 × 150 mm, 5 μM) was equilibrated with 0.05% trifluoroacetic acid in water, with a linear gradient of 0–60% acetonitrile within 40 min with a flow rate of 1 ml/min. (*B*) Differential effect of rMT-5 on mammalian and insect Na_vs expressed in *Xenopus leavis* oocytes. Representative whole cell Na^+ current traces of oocytes expressing cloned Na_vs are shown and an asterisk indicates the steady-state current peak amplitude in the presence of 1 μM toxin.

Table 2. The Efficacy (I_{30}/I_{peak}) of Recombinant MT-5 (rMT-5) and Its Mutants on $rNa_v1.1$.

Peptide	Theoretical MW (Da)	Experimental MW (Da)	I_{30}/I_{peak} of $rNa_v1.1$
rMT-5	7,171.2	7,171.4	0.60 ± 0.08
K8A	7,114.1	7,115.2	0.28 ± 0.04
P9A	7,145.2	7,146.3	0.62 ± 0.07
E15A	7,113.2	7,114.6	0.31 ± 0.05
D18A	7,127.2	7,128.3	0.09 ± 0.04
S22G	7,141.2	7,141.3	0.22 ± 0.07
I40A	7,129.1	7,129.9	N.A.
L41A	7,129.1	7,130.2	N.A.
A52K	7,228.3	7,228.9	0.44 ± 0.10
Δ19AF20	6,953.0	6,953.8	0.06 ± 0.03

NOTE.—N.A. means no activity on the tested channel with 1 μM peptide. Molecular weights (MWs) of the recombinant peptides were determined by MALDI-TOF and theoretical MWs were calculated by the compute pI/Mw tool (http://www.expasy.org/). (last accessed December 5, 2014).

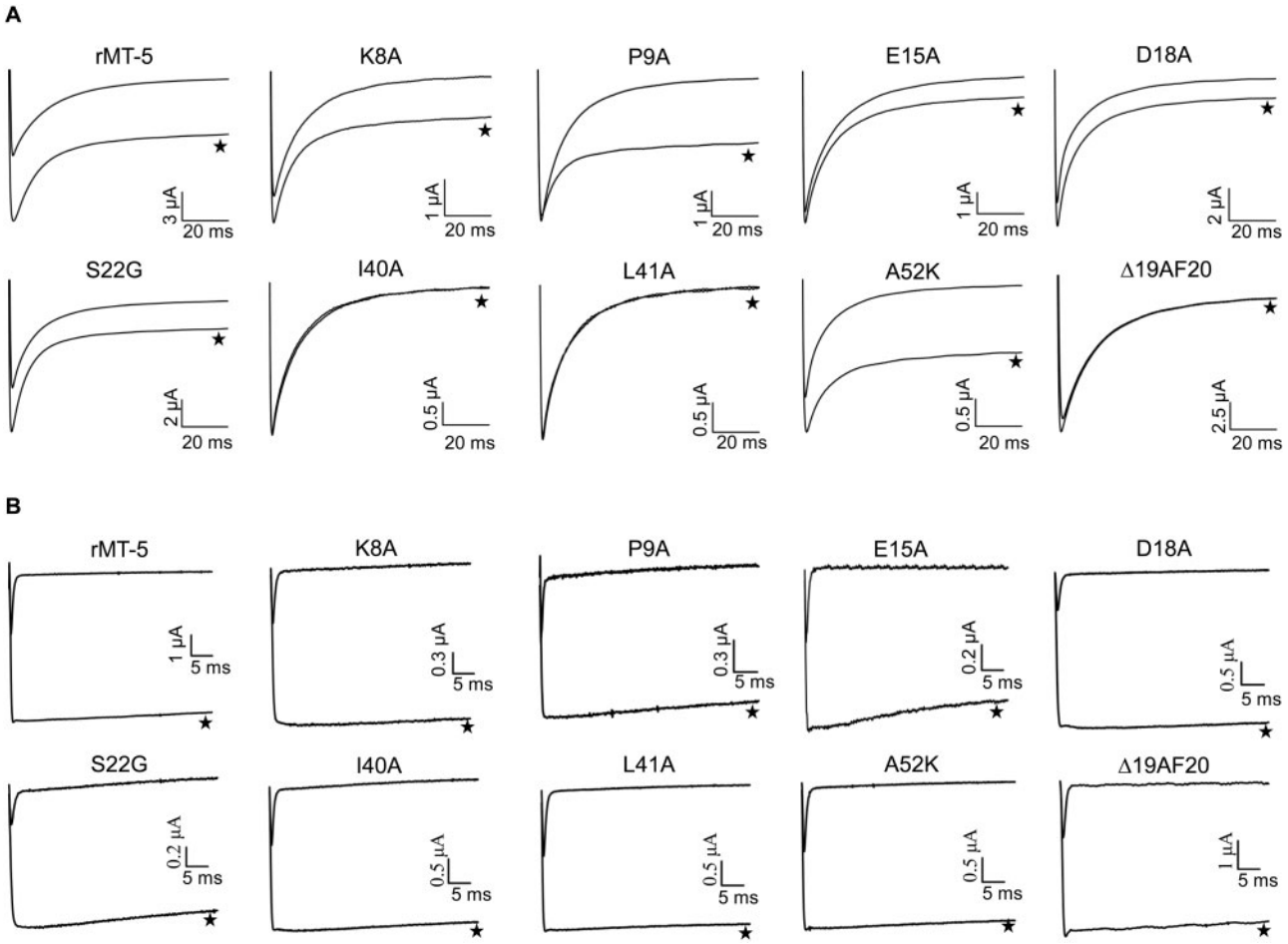

FIG. 4. The efficacy of rMT-5 and its mutants on $rNa_v1.1$ (*A*) and *Dm*Na_v1 (*B*) expressed in *X. leavis* oocytes. The steady-state currents of channels in control and after the addition of 1 μM toxin are shown. Current traces were evoked by a depolarization step to −10 mV from a holding potential of −90 mV.

Toxicity of rMT-5 and Its Mutants on Houseflies and Mice

We compared insecticidal activity of each mutant with that of rMT-5 on housefly adults. Houseflies showed typical symptoms of envenomation after peptide injection. Concentration-dependent lethality and median lethal dose (LD_{50}) values are presented in figure 7 and table 4, respectively. In our assays, rMT-5 had a LD_{50} of 0.42 nmol/g body weight that is comparable with that of the native peptide (0.20 nmol/g) (Zhu et al. 2012), both are more potent than LqhαIT, a classical insect-specific α-ScNaTx, on aphids, which had a LD_{50} of 1.14 nmol/g (Pal et al. 2013). Three mutants (D18A, I40A, and L41A) retained a relative toxicity of 19.48%, 11.68%, and 6.64% of rMT-5, respectively,

with LD_{50} values ranging from 2.17 to 6.37 nmol/g. Despite significant reduction in anti-housefly activity relative to rMT-5, these three mutants still exhibited a relatively high toxicity on houseflies when compared with U1-LITX-Lw1a, a scorpion venom-derived insecticidal peptide from *Liocheles waigiensis* that kills blowfly at a LD_{50} of 5.0 nmol/g (Smith et al. 2011). K8A, E15A, S22G, and A52K retained substantial insecticidal toxicity, 42.34%, 32%, 63.18%, and 34.60% of rMT-5, respectively (LD_{50} range: 0.67–1.32 nmol/g), while P9A displayed a similar toxicity to rMT-5 (104% of rMT-5). Unexpectedly, Δ19AF20 gained higher insect toxicity than the unmodified peptide (188% of rMT-5) with an LD_{50} of 0.23 nmol/g. The differential response to MT-5 mutants between *Drosophila* $DmNa_v1$ and housefly could be a reflection of the amino acid sequence difference in the toxin-bound region of their Na_v channels (supplementary fig. S1, Supplementary Material online). This speculation is strengthened by the previous observation that *Locusta migratoria* and *Drosophila melanogaster* both have different pharmacological properties to scorpion α-like toxins (Bosmans et al. 2005).

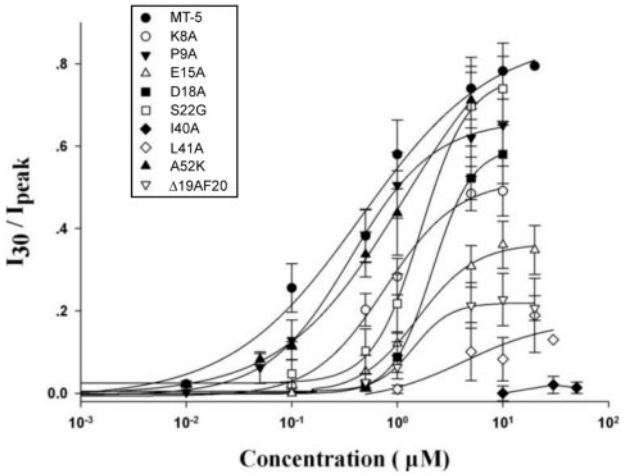

FIG. 5. Dose-response curves of rMT-5 and its mutants on $rNa_v1.1$ channel expressed in *X. laevis* oocytes. The curves were obtained by plotting the relative I_{30ms}/I_{peak} values of the channel in function of the toxin concentrations.

Table 3. Toxicity of rMT-5 and Its Mutants on Na^+ Channels.

Toxin	$rNa_v1.1$ (EC_{50}, μM)	Fold Reduction	$DmNa_v1$ (EC_{50}, μM)	Fold Reduction
MT-5	n.d.	—	0.28 ± 0.04	
rMT-5	0.45 ± 0.15	—	0.34 ± 0.05	
K8A	0.77 ± 0.12	0.71	0.30 ± 0.03	−0.12
P9A	0.36 ± 0.02	−0.2	n.d. (<1)	<1.94
E15A	1.55 ± 0.18	2.44	n.d. (<1)	<1.94
D18A	2.15 ± 0.03	3.8	0.27 ± 0.08	−0.21
Δ19AF20	>50	>110.11	0.39 ± 0.08	0.15
S22G	1.67 ± 0.27	2.71	n.d. (<1)	<1.94
I40A	>50	>110.11	n.d. (<1)	<1.94
L41A	>50	>110.11	n.d. (<1)	<1.94
A52K	1.14 ± 0.21	1.53	n.d. (<1)	<1.94

NOTE.—Fold reduction was calculated as (EC_{50} of a mutant—EC_{50} of rMT-5)/EC_{50} of rMT-5. n.d. means not determined. MT-5 is the native peptide isolated from the venom of *M. eupeus* (Zhu et al. 2012).

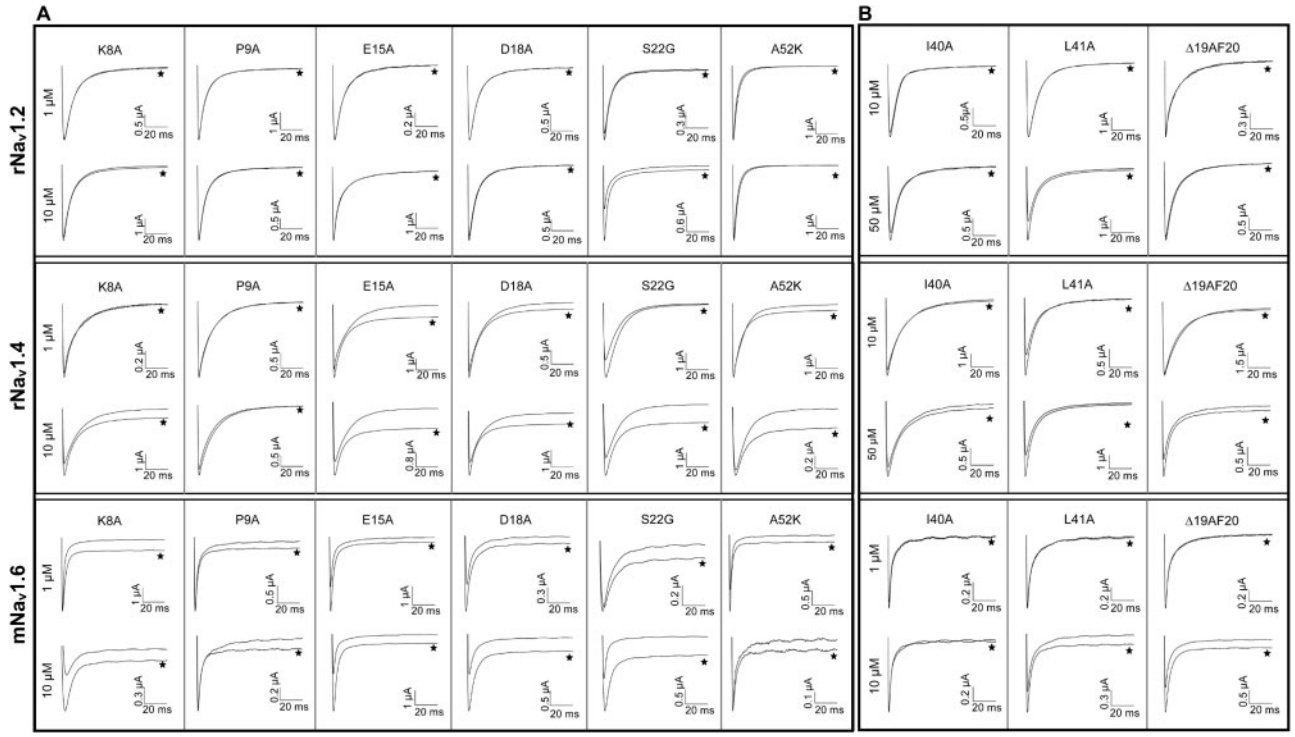

FIG. 6. Comparison of the effect of mutations at nonhot-spots (*A*) and hot-spots (*B*) on $rNa_v1.2$, $rNa_v1.4$ and $mNa_v1.6$ expressed in *X. leavis* oocytes. The steady-state currents of channels in control and after the addition toxins (asterisk) are shown. Current traces were evoked by a depolarization step to −10 mV from a holding potential of −90 mV.

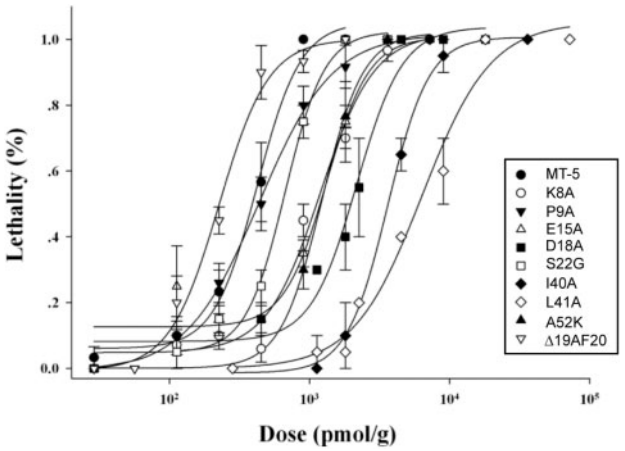

FIG. 7. Dose-response curves of rMT-5 and its mutants on insect toxicity. Insect toxicity assays performed by injecting toxins into housefly adults. All the data are presented as the mean ± SE of at least three experiments.

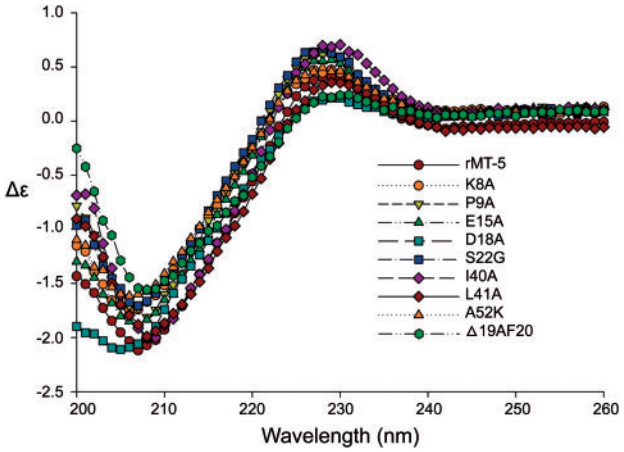

FIG. 8. CD spectra of rMT-5 and its mutants. Spectra were taken at a peptide concentration of 0.1 mg/ml.

Table 4. Toxicity of rMT-5 and Its Mutants on Housefly Adults and Mice.

Toxin	Housefly Adults (LD_{50}, nmol/g) (Mean ± SE)	Relative Toxicity (%)	Mice (LD_{50}, mg/kg) (95% Confidence Interval)	Relative Toxicity (%)
MT-5	0.20 ± 0.02	—	n.d.	
rMT-5	0.42 ± 0.04	100	0.07 (0.06–0.09)	100
K8A	1.19 ± 0.18	42.34	0.12 (0.09–0.16)	58.33
P9A	0.44 ± 0.02	96.98	0.03 (0.02–0.03)	233
E15A	1.32 ± 0.26	32.00	0.19 (0.15—0.21)	36.84
D18A	2.17 ± 0.27	19.48	0.14 (0.12—0.17)	50
Δ19AF20	0.23 ± 0.02	187.51	1.72 (1.64—1.80)	4.07
S22G	0.67 ± 0.06	63.18	0.05 (0.04—0.07)	140
I40A	3.62 ± 0.08	11.68	3.63 (3.09—5.07)	1.93
L41A	6.37 ± 1.16	6.64	5.45 (4.85—7.26)	1.28
A52K	1.22 ± 0.05	34.60	0.04 (0.03—0.05)	175

NOTE.—Relative toxicity was calculated as percentage of LD_{50} of rMT-5/LD_{50} of a mutant on housefly adults or mice.

In a previous study on the spider venom-derived neurotoxin PnTx4(5-5), it has been observed that an action on ionic channels does not necessarily means an apparent toxicity on mammals (Paiva et al. 2016). We therefore evaluated the toxicity of rMT-5 and its mutants on mice to check the consistency between in vitro and in vivo data. It was found that rMT-5 was highly active on mice with a LD_{50} of 0.07 mg/kg, 6.6-fold more active than BmKM1 (0.53 mg/kg), a major toxic component in the venom of *M. martensii* (Sun et al. 2003). The high toxicity could be attribute to its wide-spectrum of activity on multiple Na_v channel subtypes in mice, including $Na_v1.1$, $Na_v1.3$–$Na_v1.7$ (Zhu et al. 2012; this work). In contrast, PnTx4(5-5) only exhibited some activity on two channel subtypes and thus led to no detectable toxicity (Paiva et al. 2016). Consistent with the pharmacological data, at the in vivo level the three hot-spot mutants lost most of the toxicity on mice with only 1.28–4.07% activity of rMT-5 retained. The LD_{50} values are 1.72 (Δ19AF20), 3.63 (I40A), and 5.45 mg/kg (L41A), respectively, with 24- to 77-fold reduction in toxicity. In contrast, the nonhot spot mutants substantially retained the toxicity of rMT-5 from 36.84% to 58.33% and even increased to 140% (S22G), 175% (A52K), and 233% (P9A) of rMT-5 (table 4). The toxicity increase in these mutants could be related to their activity increase to certain Na_v channel subtypes, as observed in S22G on rNav1.2 (fig. 6A).

The Interaction between MT-5 and $rNa_v1.1$

To distinguish whether the observed mutational effect in MT-5 is a consequence of substitutions of functional residues rather than structural alteration in recombinant peptides, we compared the circular dichroism (CD) spectroscopy between these mutants and rMT-5. The results showed that their CD spectra were highly similar (fig. 8) and thus ruled out a potential structural impact on the function of the mutants.

To understand the structural basis of PSSs associated with toxin's potency, we built a model in which MT-5 was docked onto the VSD(DIV) of $rNa_v1.1$ via ZDOCK (fig. 9). In this complex model, the toxin binds within a crevice between two external loops S1-S2 ($L_{DIVS1-S2}$) and S3-S4 ($L_{DIVS3-S4}$) of the channel. This complex model perfectly coincides with our current and prior experimental data: 1) first, the two loops of VSD(DIV), previously characterized as a primary interaction receptor with α-ScNaTxs, and the two functionally important loops (B- and J-loop) in MT-5 characterized here, are located on the interface of the complex (fig. 9) and 2) second, four hot-spot functional residues in MT-5 (I^{40}, L^{41}, A^{19}, and F^{20}) were found to interact with channel residues previously recognized as key for toxin binding since their mutations strongly reduced toxic effect of several α-ScNaTxs (e.g., Lqh2, Lqh3, LqhαIT, and Lqq5 from *Leiurus quinquestriatus quinquestriatus*), including T^{1560} (T^{1570} in $rNa_v1.1$) and E^{1613} (E^{1623} in $rNa_v1.1$) in $rNa_v1.2$, and Y^{1433} (Y^{1628} in $rNa_v1.1$) and F^{1434} (F^{1629} in $rNa_v1.1$) in $rNa_v1.4$ (Leipold et al. 2005; Wang et al. 2011). The interacting residue pairs identified here include I^{40} and E^{1623}, L^{41} and T^{1570}, and A^{19}/F^{20} and $^{1628}Y/F^{1629}$ between MT-5 and $rNa_v1.1$ (fig. 9). The latter may form specific aromatic–aromatic interaction between the toxin-channel, as observed in the inhibitor famoxadone and its protein target ubiquinol cytochrome c oxido-reductase (Gao et al. 2002).

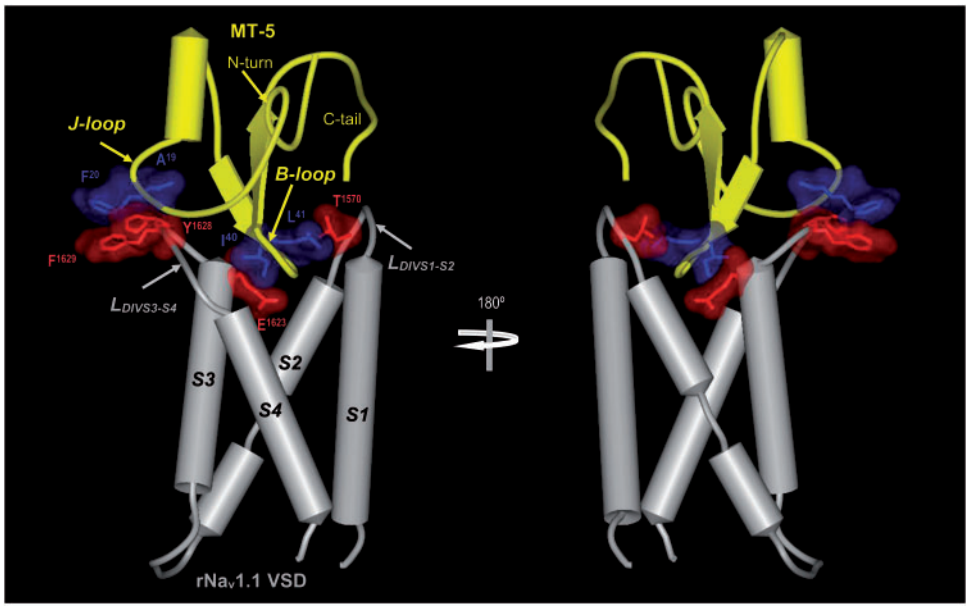

Fig. 9. A representative configuration of MT-5 in complex with the voltage-sensing domain (VSD)(DIV) of rNa$_v$1.1. Schematic representation of the complex showing functionally important residues implicated in toxin-channel interaction, all displayed as sticks covered by molecular surface ("blue," toxin; "red," channel). Two PSSs (I^{40} and L^{41}) and the insertion ($^{19}AF^{20}$) in J-loop of the toxin are predicted to bind to the previously characterized toxin-bound amino acids on Na$_v$ channels (Leipold et al. 2005; Wang et al. 2011).

MT-5 Binds to Evolutionarily Variable Sites of Na$_v$ Channels

In our previous study, we have observed that PSSs from the *M. martensii* α-ScNaTxs bind to evolutionarily variable sites of the VSD(IV) of Na$_v$ channels from prey and predators of scorpions and thus proposed the opinion of target-driven PS of scorpion toxins (Zhang et al. 2015). With the complex of MT-5 and the channel at hand, we reanalyzed the evolutionary conservation of channels from a combined data set of birds, lizards, mammals, and insects via constructing sequence logo by WebLogo (Crooks et al. 2004) and calculating conservation scores by Consurf (Armon et al. 2001). As shown in figure 10, among the hot-spot residues characterized here, two were found to interact with variable sites of the Na$_v$ channel receptor (1570 and 1623) (fig. 10), in which site 1570 is occupied by D/E/I/K/N/Q/S/T/V and 1623 by A/D/E/G/K/Q/T, which match PSSs 41 and 40, respectively. In the two sibling scorpion species (*M. epeus* and *M. martensii*), these two toxin sites are occupied by I/L/Q/W/Y and A/F/G/L/Q/V/W, respectively. These observations indicate that toxins' mutations at these two functional sites will be fixed by PS if a mutation fits a residue in the two corresponding positions of the channels. However, different from the two evolutionarily variable channel sites, Y^{1628} and F^{1629} targeted by A^{19} and F^{20} are highly conserved. This could suggest that this species-specific insertion has potential to affect more channel subtypes via trapping a conserved region.

Discussion

Functional Significance of PSSs

Among the eight PSSs, two (I40A and L41A) are characterized as the most crucial amino acid sites whose mutations resulted in activity loss of MT-5 to multiple Na$_v$ channel subtypes and profound reduction of toxicity on houseflies and mice. Consistently, they were recognized as hot-spot residues in the complex model (fig. 9). In previous experiments site 40 (equivalent to site 39 in Lqh3 and 38 in others) has been identified as functional residues in other α-ScNaTxs (e.g., AaH2, BmKM1, Lqh2, Lqh3, and LqhαIT) (Kharrat et al. 1989; Sun et al. 2003; Karbat et al. 2004, 2007; Bosmans and Tytgat 2007; Kahn et al. 2009). Substitutions or sulfenylation of Trp or Phe at this site all resulted in decreased toxicity on mammals and insects and their Na$_v$ channels. Notwithstanding, this site was not predicted as a PSS in two previous publications (Zhu et al. 2004; Weinberger et al. 2010). It appears that this site is only positively selected in the *Mesobuthus* lineage because in our recent analysis of the *M. martensii* α-ScNaTxs, this site was again recognized as a PSS (Zhang et al. 2015), indicating a lineage-specific accelerated evolution pattern.

Site 41 is a common PSS predicted from different data sets (Zhu et al. 2004, 2012; Weinberger et al. 2010; Zhang et al. 2015). In the work of Weinberger et al. (2010), substitution of A^{39} by a Leu in LqhαIT and Lqh2 (equivalent to site 41 in MT-5) not only increased their activity but also rendered LqhαIT active on rNa$_v$1.2, and Lqh2 active on *Dm*Na$_v$1. Reverse mutation from Leu to Ala in MT-5 resulted in deprivation of its activity on mammalian Na$_v$ channels and substantial toxicity decrease on mice but no effect on the *Drosophila* Na$_v$ channels. These observations demonstrate that a more hydrophobic side-chain at this site is favored for toxicity on mammals and some insects.

Our mutagenesis experiments confirmed the functional importance of two PSSs (E^{15} and D^{18}) whose mutations reduced the activity of MT-5 on mice and houseflies. In fact,

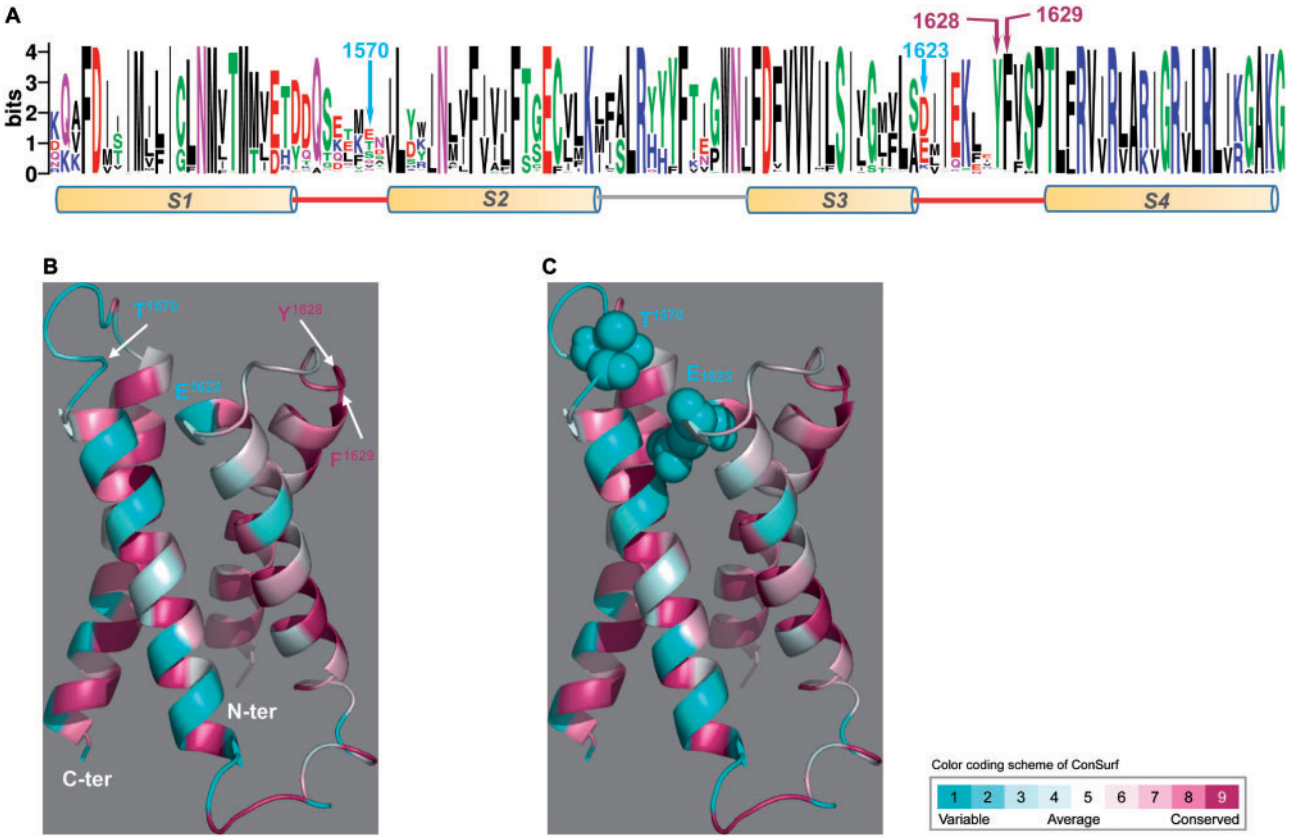

Fig. 10. Evolutionary conservation and variability of the VSD(DIV) in prey and predators of scorpions. (*A*) Sequence logo. The logo was constructed from a total of 184 Na_v channels from mammals, birds, lizards, and insects (Zhang et al. 2015). Each logo consists of stacks of letters and the overall height of each stack indicates the sequence conservation at that position (measured in bits). The height of symbols within the stack reflects the relative frequency of the corresponding amino acid at that position. Secondary structure elements were extracted from the model of $rNa_v1.1$. Arrows in "cyan" indicate the channel residues that bind to the two PSSs (I^{40} and L^{41}), and arrows in "purple" indicate the channel residues interacting with the small insertion (19AF20). The residues are numbered according to $rNa_v1.1$; (*B*) High variability of scorpion α-toxin-bound regions in Na_v channels from both predators and prey of scorpions, with two key toxin-bound sites amino acids (T^{1570} and E^{1623}) in $rNa_v1.1$ shown in sphere models (***C***).

substitution R^{18} in LqhαIT and Lqh2 or P^{18} in Lqh3 also caused significantly decreased activity on insect and/or mammalian Na_v channels (Karbat et al. 2004, 2007; Kahn et al. 2009). However, the functional role of site 15 is a bit complex. Mutation at this site affected the activity of Lqh3, Lqh2, and AaH2 (Karbat et al. 2007; Kahn et al. 2009; Chen and Chung 2012), but did not affect the activity of LqhαIT or BmKM1 (Zilberberg et al. 1997; Sun et al. 2003; Wang et al. 2003; Karbat et al. 2004; Liu et al. 2005). The functional significance of site 22 of α-ScNaTxs has remained unclear. Our data highlight a role of site S^{22} in binding of MT-5 to mammalian other than insect Na_v channels.

Similar to site 15, the function of sites 8 and 9 is also bipolar. Mutations of these two sites in BmKM1, LqhαIT, Lqh2, and Lqh3 led in differential impact upon the activity (Ye et al. 2005; Karbat et al. 2007; Schnur et al. 2008; Kahn et al. 2009). In BmKM1, they are considered as a molecular switch regulating species selectivity of the toxin (Ye et al. 2005) and are also involved in LqhαIT binding to insect Na_v channels (Schnur et al. 2008). However, substitutions of these two sites in Lqh2 and Lqh3 resulted in no significant effect on the toxin activity (Karbat et al. 2007; Kahn et al. 2009). In MT-5, sites 8 and 9 were not implicated in binding to $rNa_v1.1$ and $mNa_v1.6$, as in the case of Lqh2 and Lqh3, however, mutations at these two sites led to the reduction of activity on $rNa_v1.4$ (fig. 6), suggesting its differential contributions to toxin binding to different channel subtypes.

Functional Significance of the Insertion

Indel (insertion and deletion) is a common type of sequence mutation in protein evolution and can induce a high substitution rate in its flanking regions (Tian, Wang, et al. 2008). A key role of indels in toxic origin of peptide and protein scaffolds has been reported previously (Aminetzach et al. 2009; Zhu et al. 2014; Zhang et al. 2016). In comparison with α-ScNaTxs from other species, the MeuNaTxα multigene family members contain a species-specific small insertion ranging from two to eight residues in their J-loop (Zhu et al. 2012; fig. 2). Our mutational analysis has characterized two PSSs (D^{18} and S^{22}) in this region, which are associated with the toxin's function. We found that a two-residue deletion (19AF20) in this positively selected loop induced a dramatic functional switch from an α-like toxin to an overall insect-specific toxin. This is the first report on the role of a small

insertion in toxin functional diversification in the α-ScNaTx family. Despite technical limitation in identification of PS due to the lack of plenty of toxin sequences containing an insertion, the functional importance along with its unique location in a positively selected loop suggests that this class of mutation was evolutionarily favored.

Target-Driven PS of Toxins

Despite remarkable progress in identifying PS of α-ScNaTxs, a full understanding of their adaptive evolution cannot be achieved without considering the selective agents responsible for PS. Two mechanisms have been proposed to account for driving forces of PS in proteins (i.e., agent of selection): 1) external mechanisms, such as adaptation to different ecological niches and 2) internal mechanisms, such as coevolution between receptor and ligand, and compensatory mutations within a molecule (MacColl 2011; Morgan et al. 2012). Our recent studies have suggested that an essential agent of selection for α-ScNaTxs comes from the evolutionarily variability of receptor site of Na_v channels from predators and prey of scorpions (Zhang et al. 2015). This represents an external mechanism driving PS of the scorpion toxins. The observation that the two hot-spot PSSs (I^{40} and L^{41}) respectively interact with two highly variable channel sites (1623 and 1570) (figs. 9 and 10) in our toxin-channel complex model further strengthens our previous opinion that the evolution of scorpion toxins is driven by their targets (Zhang et al. 2015).

In addition to the complex model described here, other three models of toxins (AaH2, Lqh2, and BmKM1) in complex with the VSD(DIV) of $rNa_v1.2$ have also been published (Wang et al. 2011; Chen and Chung 2012; Zhang et al. 2015). Overall, these three models predicted similar interface between the toxins and the channel, similar to that between MT-5 and $rNa_v1.1$ (fig. 9). However, residues of each toxin in the interface exhibited some differences. Such discrepancy may be attributed to their differential functional surfaces. For example, the N-turn whose functional importance has been revealed in BmKM1 and LqhαIT, but not in Lqh2 and Lqh3 as well as MT-5 for $rNa_v1.1$. In the latter three toxins, this region is far from the interface of toxin-channel complexes. In the AaH2-$Na_v1.2$ VSD(DIV) complex, Arg^{18} and Trp^{38} of AaH2 are predicted to bind to Glu^{1613} and a cluster of hydrophobic residues (e.g., Tyr^{1564} and Trp^{1565}) of the channel, respectively. In the Lqh2-$Na_v1.2$ VSD(DIV) complex, Glu^{1613} is predicted to bind to Asn^{44} of the toxin. In MT-5, these two residues are structurally equivalent to Asp^{18} and Ile^{40}, respectively, in which Asp^{18} is in close proximity to K^{1627}–V^{1630} of $rNa_v1.1$, a continuous region known to be involved in toxin binding (Bosmans and Tytgat 2007). Another possibility for the discrepancy could result from the difference in the Na_v channel structures due to the use of different templates. When compared with the previous channel models (Wang et al. 2011; Chen and Chung 2012), our model shows the smallest root-mean-square deviation with the experimental structure of *Ci*-VSD (Li et al. 2014; supplementary fig. S2, Supplementary Material online).

MT-5 Mutants Are Promising Candidate Insecticides

High-level expression of insect-specific scorpion sodium channel toxins in insecticidal fungi has been proven to be a promising method in pest control (Wang and St Leger 2007). As mentioned previously, MT-5 is an α-like toxin with a wide-spectrum channel activity (Zhu et al. 2012). In our assays, a deletion mutation (19AF20) in the positively selected J-loop of MT-5 significantly impaired its anti-mammalian activity but substantially enhanced its insecticidal activity. For I40A and L41, their anti-mammalian activity was remarkably reduced and only 1.28–1.93% of rMT-5 toxicity retained whereas their anti-housefly activity retained 6.64–11.68% of the unmodified peptide (table 4). In particular, these two mutants displayed comparable insect toxicity with U1-LITX-Lw1a (Smith et al. 2011), as mentioned previously, and MeuNaTxα-13 (LD_{50} of 5.3 nmol/g to houseflies) (Zhu et al. 2013). Therefore, mutations at these hot-spots led to a functional switch of MT-5 from an α-like toxin to anti-insect α-toxins (i.e., highly toxic to insects but weakly potent to mammals) (Zhu et al. 2012). Taken together, our results demonstrate that these new mutants could have a potential as promising candidate insecticide leads. Saturation mutagenesis (Reetz and Carballeira 2007) at these sites to introduce new side-chains and further adjust MT-5's insect and mammalian selectivity is under way.

Conclusion and Perspectives

In this study, we systematically evaluated the functional significance of eight newly characterized PSSs of α-ScNaTxs from the *Mesobuthus* lineage via mutational analysis. The mutagenesis data presented here reveal differential contributions of PSSs to a specific toxin in interacting with different Na_v channels and also suggest some differences in binding pattern among toxins toward a specific channel. Furthermore, the data allow to define the functional surface of an α-like toxin interacting with $rNa_v1.1$, in which the J-loop and B-loop are highlighted as directly being implicated in toxin binding and species selectivity. Our results clearly show that mutations at hot-spots can reduce the effect of α-ScNaTxs on mammalian Na_v channels without changing the effect on *Drosophila* Na_v channel, which shifts the selectivity ratio of MT-5 toward insects. The difference in toxin sensitivity to rMT-5 mutants among insect species (e.g., *Drosophila* and houseflies) highlights a key role of PSSs in evolution-guided design of novel Na_v channel-targeted molecules with improved potency and phylogenetic selectivity, even against a specific pest species without affecting beneficial insects. Meanwhile, the results also indicate that MT-5 could serve as a potential lead for insecticides since its anti-mammalian activity could be easily manipulated by mutagenesis at PSSs and their adjacent regions (e.g., I^{40}, L^{41}, and $^{18}AF^{19}$).

Finally, one key point that still needs to be addressed in the future is how a toxin residue at a PSS was evolutionarily fixed by selection from a specific channel residue. Such a study will help to establish an interaction map of residue pairs between the toxins and their targets and improve our understanding of evolution of scorpions and their toxins. In the light hereof,

we should extend the usage of Na_v channels from two main predators of scorpions (birds and lizards) and continue trying to elucidate the molecular interactions of the toxin-channel complex in combination with saturation mutational analyses of both toxins and channels.

Materials and Methods

Construction of Expression Vectors

Primers used are listed in table 1. To insert *MT-5* into pET-28a, a forward primer (MeuNaTxα12/13-F) containing an *Nco* I restriction site and a reverse primer (MeuNaTxα13-R) containing a *Sal* I site and a stop codon were designed, making the toxin-coding region immediately juxtaposed to the initial codon of pET-28a. The *MT-5* cDNA previously reported (Zhu et al. 2012) was used as template for PCR. To construct recombinant plasmid pET-28a-MT-5, PCR product was firstly ligated into pGM-T and sequenced by T7, and then the confirmed recombinant plasmid was digested with *Nco* I and *Sal* I to release the insert for ligation into pET-28a.

Site-Directed Mutagenesis

Inverse PCR was used to prepare all mutants with pET-28a-MT-5 as template. 5′-End phosphorylation of primers was performed with T4 polynucleotide kinase (TOYOBO, Osaka) and ATP (Takara, Dalian). ExTaq DNA polymerase (Takara, Dalian) was used to amplify the full-length pET-28a-MT-5 by two back-to-back primers, one of which contained the required mutation (table 1). Subsequently, linear PCR product was circularized by T4 DNA ligase (Takara, Dalian) following end polishing by Pfu polymerase (newProbe, Beijing). Circularized products were transformed into *E. coli* DH5α competent cells. Positive clones were confirmed by DNA sequencing.

Preparation and Identification of Recombinant Products

Expression, refolding and purification of recombinant MT-5 (rMT-5) and its mutants were performed according to the method previously described (Turkov et al. 1997; Zhu et al. 2013). In brief, a recombinant plasmid was transformed into *E. coli* BL21(DE3)pLysS cells. The induction was initiated by adding 0.5 mM Isopropyl β-D-1-Thiogalactopyranoside at an OD_{600} of 0.3. Cells were harvested 4 h later by centrifugation and pellets were resuspended in Resuspension Buffer (0.1 M Tris-HCl, pH 8.5; 0.1 M NaCl) for cell disruption by sonication.

All recombinant proteins studied were accumulated as inclusion bodies and were refolded according to the following procedures: inclusion bodies were firstly washed with Isolation Buffer (2 M urea and 2% Triton X-100 in Resuspension Buffer) and then solubilized in Denaturation Solution containing 6 M guanidine-HCl, 0.1 M Tris-HCl (pH 8.5), 1 mM ethylene diamine tetraacetic acid, and 30 mM β-mercaptoethanol for 2 h. Refolding was initiated by 20-fold dilution in 0.2 M ammonium acetate (pH 9.0) at room temperature for 48 h and the precipitates were removed by filter. Refolded proteins were recovered by salting out at 80% saturation of solid ammonium sulfate. The precipitates were collected and dissolved in water.

Recombinant peptides were further purified by RP-HPLC and effluent was monitored at the absorbance of 225 nm. Fractions eluted were collected for sodium dodecyl sulfate–polyacrylamide gel electrophoresis. Molecular weights of recombinant products were determined by MALDI-TOF mass spectrometry and their secondary structures were studied by CD spectroscopy analysis on a Chirascan Plus spectropolarimeter (UK). Peptides were dissolved in 5 mM sodium phosphate buffer (pH 7.0) at a concentration of 0.1 mg/ml. Spectra were measured from 260 to 200 nm by using a quartz cell of 1.0 mm thickness. Data were collected at 1 nm intervals with a scan rate of 60 nm/min and expressed as molar CD (delta epsilon), calculated as follows: $\Delta\varepsilon = [\theta \times (0.1 \times MRW)/(L \times C)]/3{,}298.2$, where θ is the ellipticity (in millidegrees), C is the concentration (in mg/ml), L is the pathlength (in cm), and MRW is the mean residue weight (in Da).

Electrophysiological Recordings

For expression of Na_v channels ($rNa_v1.1$, $rNa_v1.2$, $rNa_v1.4$, $rNa_v1.5$, $mNa_v1.6$, and $DmNa_v1$/TipE) in *Xenopus* oocytes, linearized plasmids were transcribed by mMESSAGE-mMACHINE transcription kits (Ambion, USA). The harvesting of stage V-VI oocytes from anesthetized female *Xenopus laevis* was described previously (Zhu et al. 2013). Oocytes were injected with Na_v channel cRNAs using a micro-injector (Nanoliter 2000, WPI) and then incubated in ND96 solution with 50 mg/l gentamycin sulfate at 16 °C for 1–5 days.

Two-electrode voltage-clamp recordings were performed at room temperature with an Oocyte Clamp Amplifier (OC-725C, Harvard Apparatus Company) controlled by a data acquisition system (Digidata 1440A, Axon CNS) dominated by pCLAMP 10.2. Leak subtraction was performed by a -P/4 protocol. Resistances of both electrodes were kept at 0.5–1.5 MΩ. The elicited currents were filtered at 1 kHz and sampled at 20 kHz with a four-pole low-pass Bessel filter.

The dose-response effect of toxins (slowing down of inactivation) was calculated by plotting the ratio of the steady-state current measured 30 ms (I_{30ms}) after depolarization to the control peak current (I_{peak}) as a function of toxin concentration. The data were fitted with the Hill equation. Data were shown as means ± standard error (SE) of at least three independent experiments and analyzed by SigmaPlot 11.0.

Toxicity Assays

Insecticidal activity was measured by injecting peptides dissolved in insect saline (200 mM NaCl, 3.1 mM KCl, 5.4 mM $CaCl_2$, 5 mM $MgCl_2$, 2 mM $NaHCO_3$, 0.1 mM NaH_2PO_4, pH 7.2) (Wang et al. 1999) into housefly adults, as described previously (Wang et al. 1999; Tedford et al. 2001). Experiments were performed in triplication with a cohort of ten flies for each concentration of the toxins. Control flies were injected with 1 μl of insect saline. All flies were kept at 4 °C during injection and subsequently transferred to room temperature. The LD_{50} was calculated by SigmaPlot 11.0 that fitted the dose-response data with the Hill equation, $y = (a-b)/[1+(x/LD_{50})^n]+b$, where "$y$" represents the

percentage of deaths in the sample population at 12 h post-injection, "*x*" represents the toxin dose in pmol/g, "*n*" is the variable slope factor, "*a*" is maximum response, and "*b*" is minimum response. For mouse toxicity assay, rMT-5 and its mutants were dissolved in 0.9% NaCl at five different doses for each toxin and injected into SPF (Specific Pathogen-Free) mice through the tail vein. Each group contained ten mice (about 25 g of body weight/mouse). Numbers of dead mice were recorded at 24 h post-injection. LD_{50} was calculated according to Bliss mothed implemented in SPSS Statistics 17.0.1 (SPSS Inc.).

Molecular Docking

Structures of $rNa_v1.1$ VSD(DIV) (residues 1540–1655) were built based on the crystal structures of the *Ciona intestinalis* VSD (*Ci*-VSD) in active or rest conformation (pdb entries 4G7V and 4G80) (Li et al. 2014; supplementary fig. S3, Supplementary Material online). ZDOCK (version 3.0.2), a Fast Fourier transform (FFT)-based, rigid-body protein-protein docking program (Pierce et al. 2014) (http://zdock.umassmed.edu/, last accessed June 25, 2015), was employed to construct the complex model. ZDOCK searches all possible binding modes in the translational and rotational space between the two proteins and performs scoring calculations based on a combination of statistical potential of interface atomic contact energies, shape complementarity, and electrostatics (Mintseris et al. 2007). The atom coordinates of MT-5 (pdb entry 2LKB) and the $rNa_v1.1$ VSD(DIV) structure in its rest state were used as inputs for ZDOCK calculations. On the basis of our mutagenesis data from MT-5 in combination with previous data from Na_v channel mutations (Leipold et al. 2005; Wang et al. 2011), we specified binding site residues for filtering output predictions, which include sites 19, 20, 40, and 41 in MT-5 and sites 1570, 1623, 1627–1630 in the VSD(DIV) of $rNa_v1.2$ and $rNa_v1.4$ (numbered according to $rNa_v1.1$), which all are associated with the toxin-channel interaction. Docking of the VSD(DIV) of $rNa_v1.1$ in its active state with MT-5 generated similar solutions (data not shown).

Supplementary Material

Supplementary figures S1–S3 and table S1 are available at *Molecular Biology and Evolution* online (http://www.mbe.oxfordjournals.org/).

Acknowledgments

The authors wish to acknowledge the anonymous reviewers for their valuable comments to the manuscript. This work was supported by the National Natural Science Foundation of China (31570773) and the State Key Laboratory of Integrated Management of Pest Insects and Rodents (Grant No. ChineseIPM1512) to S.Z.; J.T. was supported in part by FWO-Vlaanderen grant G.0E34.14, IUAP 7/10 (Inter-University Attraction Poles Program, Belgian State, Belgian Science Policy) and OT/12/081 (KU Leuven).

References

Aminetzach YT, Srouji JR, Kong CY, Hoekstra HE. 2009. Convergent evolution of novel protein function in shrew and lizard venom. *Curr Biol*. 19:1925–1931.

Armon A, Graur D, Ben-Tal N. 2001. ConSurf: an algorithmic tool for the identification of functional regions in proteins by surface mapping of phylogenetic information. *J Mol Biol*. 307:447–463.

Bosmans F, Brône B, Sun YM, Zhu RH, Xiong YM, Wang DC, Van Kerkhove E, Tytgat J. 2005. Pharmacological comparison of two different insect models using the scorpion α-like toxin BmKM1 from *Buthus martensill Karsch*. *Protein Pept Lett*. 12:363–367.

Bosmans F, Tytgat J. 2007. Voltage-gated sodium channel modulation by scorpion α-toxins. *Toxicon* 49:142–158.

Catterall WA, Goldin AL, Waxman SG. 2005. International Union of Pharmacology. XLVII. Nomenclature and structure-function relationships of voltage-gated sodium channels. *Pharmacol Rev*. 57:397–409.

Cestele S, Catterall WA. 2000. Molecular mechanisms of neurotoxin action on voltage-gated sodium channels. *Biochimie* 82:883–892.

Chen R, Chung SH. 2012. Binding modes and functional surface of antimammalian scorpion α-toxins to sodium channels. *Biochemistry* 51:7775–7782.

Crooks GE, Hon G, Chandonia JM, Brenner SE. 2004. WebLogo: a sequence logo generator. *Genome Res*. 14:1188–1190.

Duda TF Jr, Palumbi SR. 1999. Molecular genetics of ecological diversification: duplication and rapid evolution of toxin genes of the venomous gastropod *Conus*. *Proc Natl Acad Sci U S A*. 96:6820–6823.

Duda TF Jr, Palumbi SR. 2000. Evolutionary diversification of multigene families: allelic selection of toxins in predatory cone snails. *Mol Biol Evol*. 17:1286–1293.

Gao X, Wen X, Yu C, Esser L, Tsao S, Quinn B, Zhang L, Yu L, Xia D. 2002. The crystal structure of mitochondrial cytochrome bc1 in complex with famoxadone: the role of aromatic-aromatic interaction in inhibition. *Biochemistry* 41:11692–11702.

Gordon D, Gurevitz M. 2003. The selectivity of scorpion α-toxins for sodium channel subtypes is determined by subtle variations at the interacting surface. *Toxicon* 41:125–128.

Gordon D, Karbat I, Ilan N, Cohen L, Kahn R, Gilles N, Dong K, Stuhmer W, Tytgat J, Gurevitz M. 2007. The differential preference of scorpion α-toxins for insect or mammalian sodium channels: implications for improved insect control. *Toxicon* 49:452–472.

Hill RE, Hastie ND. 1987. Accelerated evolution in the reactive centre regions of serine protease inhibitors. *Nature* 326:96–99.

Hughes AL, Nei M. 1988. Pattern of nucleotide substitution at major histocompatibility complex class I loci reveals overdominant selection. *Nature* 335:167–170.

Jover E, Couraud F, Rochat H. 1980. Two types of scorpion neurotoxins characterized by their binding to two separate receptor sites on rat brain synaptosomes. *Biochem Biophys Res Commun*. 95:1607–1614.

Juárez P, Comas I, González-Candelas F, Calvete JJ. 2008. Evolution of snake venom disintegrins by positive Darwinian selection. *Mol Biol Evol*. 25:2391–2407.

Kahn R, Karbat I, Ilan N, Cohen L, Sokolov S, Catterall WA, Gordon D, Gurevitz M. 2009. Molecular requirements for recognition of brain voltage-gated sodium channels by scorpion α-toxins. *J Biol Chem*. 284:20684–20691.

Karbat I, Frolow F, Froy O, Gilles N, Cohen L, Turkov M, Gordon D, Gurevitz M. 2004. Molecular basis of the high insecticidal potency of scorpion α-toxins. *J Biol Chem*. 279:31679–31686.

Karbat I, Kahn R, Cohen L, Ilan N, Gilles N, Corzo G, Froy O, Gur M, Albrecht G, Heinemann SH, et al. 2007. The unique pharmacology of the scorpion α-like toxin Lqh3 is associated with its flexible C-tail. *FEBS J*. 274:1918–1931.

Kharrat R, Darbon H, Rochat H, Granier C. 1989. Structure/activity relationships of scorpion α-toxins. Multiple residues contribute to the interaction with receptors. *Eur J Biochem*. 181:381–390.

Kozminsky-Atias A, Zilberberg N. 2012. Molding the business end of neurotoxins by diversifying evolution. *FASEB J*. 26:576–586.

Leipold E, Hansel A, Olivera BM, Terlau H, Heinemann SH. 2005. Molecular interaction of δ-conotoxins with voltage-gated sodium channels. *FEBS Lett*. 579:3881–3884.

Li Q, Wanderling S, Paduch M, Medovoy D, Singharoy A, McGreevy R, Villalba-Galea CA, Hulse RE, Roux B, Schulten K, et al. 2014. Structural mechanism of voltage-dependent gating in an isolated voltage-sensing domain. *Nat Struct Mol Biol*. 21:244–252.

Liu LH, Bosmans F, Maertens C, Zhu RH, Wang DC, Tytgat J. 2005. Molecular basis of the mammalian potency of the scorpion α-like toxin, BmKM1. *FASEB J*. 19:594–596.

MacColl AD. 2011. The ecological causes of evolution. *Trends Ecol Evol*. 26:514–522.

Mintseris J, Pierce B, Wiehe K, Anderson R, Chen R, Weng Z. 2007. Integrating statistical pair potentials into protein complex prediction. *Proteins* 69:511–520.

Morgan CC, Shakya K, Webb A, Walsh TA, Lynch M, Loscher CE, Ruskin HJ, O'Connell MJ. 2012. Colon cancer associated genes exhibit signatures of positive selection at functionally significant positions. *BMC Evol Biol*. 12:114.

Paiva AL, Matavel A, Peigneur S, Cordeiro MN, Tytgat J, Diniz MR, de Lima ME. 2016. Differential effects of the recombinant toxin PnTx4(5-5) from the spider *Phoneutria nigriventer* on mammalian and insect sodium channels. *Biochimie* 121:326–335.

Pal N, Yamamoto T, King GF, Waine C, Bonning B. 2013. Aphicidal efficacy of scorpion- and spider-derived neurotoxins. *Toxicon* 70:114–122.

Pierce BG, Wiehe K, Hwang H, Kim BH, Vreven T, Weng Z. 2014. ZDOCK Server: interactive docking prediction of protein-protein complexes and symmetric multimers. *Bioinformatics* 30:1771–1773.

Polis GA. 1990. *The Biology of scorpions*. Stanford (CA): Stanford University Press.

Possani LD, Becerril B, Delepierre M, Tytgat J. 1999. Scorpion toxins specific for Na^+-channels. *Eur J Biochem*. 264:287–300.

Puillandre N, Watkins M, Olivera BM. 2010. Evolution of *Conus* peptide genes: duplication and positive selection in the A-superfamily. *J Mol Evol*. 70:190–202.

Reetz MT, Carballeira JD. 2007. Iterative saturation mutagenesis (ISM) for rapid directed evolution of functional enzymes. *Nat Protoc*. 2:891–903.

Schnur E, Turkov M, Kahn R, Gordon D, Gurevitz M, Anglister J. 2008. NMR analysis of interaction of LqhαIT scorpion toxin with a peptide corresponding to the D4/S3-S4 loop of insect para voltage-gated sodium channel. *Biochemistry* 47:911–921.

Smith JJ, Hill JM, Little MJ, Nicholson GM, King GF, Alewood PF. 2011. Unique scorpion toxin with a putative ancestral fold provides insight into evolution of the inhibitor cystine knot motif. *Proc Natl Acad Sci U S A*. 108:10478–10483.

Sun YM, Bosmans F, Zhu RH, Goudet C, Xiong YM, Tytgat J, Wang DC. 2003. Importance of the conserved aromatic residues in the scorpion α-like toxin BmKM1. *J Biol Chem*. 278:24125–24131.

Tedford HW, Fletcher JI, King GF. 2001. Functional significance of the β-hairpin in the insecticidal neurotoxin ω-atracotoxin-Hv1a. *J Biol Chem*. 276:26568–26576.

Tian C, Yuan Y, Zhu S. 2008. Positively selected sites of scorpion depressant toxins: possible roles in toxin functional divergence. *Toxicon* 51:555–562.

Tian D, Wang Q, Zhang P, Araki H, Yang S, Kreitman M, Nagylaki T, Hudson R, Bergelson J, Chen JQ. 2008. Single-nucleotide mutation rate increases close to insertions/deletions in eukaryotes. *Nature* 455:105–108.

Turkov M, Rashi S, Noam Z, Gordon D, Ben Khalifa R, Stankiewicz M, Pelhate M, Gurevitz M. 1997. *In vitro* folding and functional analysis of an anti-insect selective scorpion depressant neurotoxin produced in *Escherichia coli*. *Protein Expr Purif*. 10:123–131.

Vonk FJ, Casewell NR, Henkel CV, Heimberg AM, Jansen HJ, McCleary RJ, Kerkkamo HM, Vos RA, Guerreiro I, Calvete JJ, et al. 2013. The king cobra genome reveals dynamic gene evolution and adaptation in the snake venom system. *Proc Natl Acad Sci U S A*. 110:20651–20656.

Wang C, Gilles N, Hamon A, Le Gall F, Stankiewicz M, Pelhate M, Xiong Y, Wang D, Chi C. 2003. Exploration of the functional site of a scorpion α-like toxin by site-directed mutagenesis. *Biochemistry* 42:4699–4708.

Wang C, St Leger RJ. 2007. A scorpion neurotoxin increases the potency of a fungal insecticide. *Nat Biotechnol*. 25:1455–1456.

Wang J, Yarov-Yarovoy V, Kahn R, Gordon D, Gurevitz M, Scheuer T, Catterall WA. 2011. Mapping the receptor site for α-scorpion toxins on a Na^+ channel voltage sensor. *Proc Natl Acad Sci U S A*. 108:15426–15431.

Wang X, Jimenez-Vargas JM, Xu C, Possani LD, Zhu S. 2012. Positive selection-guided mutational analysis revealing two key functional sites of scorpion ERG K^+ channel toxins. *Biochem Biophys Res Commun*. 429:111–116.

Wang X, Smith R, Fletcher JI, Wilson H, Wood CJ, Howden ME, King GF. 1999. Structure-function studies of ω-atracotoxin, a potent antagonist of insect voltage-gated calcium channels. *Eur J Biochem*. 264:488–494.

Weinberger H, Moran Y, Gordon D, Turkov M, Kahn R, Gurevitz M. 2010. Positions under positive selection–key for selectivity and potency of scorpion α-toxins. *Mol Bio Evol*. 27:1025–1034.

Wong ES, Belov K. 2012. Venom evolution through gene duplications. *Gene* 496:1–7.

Ye X, Bosmans F, Li C, Zhang Y, Wang D-C, Tytgat J. 2005. Structural basis for the voltage-gated Na^+ channel selectivity of the scorpion α-like toxin BmK M1. *J Mol Biol*. 353:788–803.

Zhang S, Gao B, Zhu S. 2015. Target-driven evolution of scorpion toxins. *Sci Rep*. 5:14973.

Zhang S, Gao B, Zhu S. 2016. Independent origins of scorpion toxins affecting potassium and sodium channels. Evolution of venomous animals and their toxins. Doi: 10.1007/978-94-007-6727-0_12-1. Springer Science + Business Media Dordrecht, Berlin, Heidelberg, Germany.

Zhu L, Peigneur S, Gao B, Tytgat J, Zhu S. 2013. Two recombinant α-like scorpion toxins from *Mesobuthus eupeus* with differential affinity toward insect and mammalian Na^+ channels. *Biochimie* 95:1732–1740.

Zhu S, Bosmans F, Tytgat J. 2004. Adaptive evolution of scorpion sodium channel toxins. *J Mol Evol*. 58:145–153.

Zhu S, Gao B, Tytgat J. 2005. Phylogenetic distribution, functional epitopes and evolution of the CSαβ superfamily. *Cell Mol Life Sci*. 62:2257–2269.

Zhu S, Peigneur S, Gao B, Lu X, Cao C, Tytgat J. 2012. Evolutionary diversification of *Mesobuthus* α-scorpion toxins affecting sodium channels. *Mol Cell Proteomics*. 11:M111.012054.

Zhu S, Peigneur S, Gao B, Umetsu Y, Ohki S, Tytgat J. 2014. Experimental conversion of a defensin into a neurotoxin: implications for origin of toxic function. *Mol Biol Evol*. 31:546–559.

Zilberberg N, Froy O, Loret E, Cestele S, Arad D, Gordon D, Gurevitz M. 1997. Identification of structural elements of a scorpion α-neurotoxin important for receptor site recognition. *J Biol Chem*. 272:14810–14816.